

March 26, 2023, a12Cwarsapw_ver6

The S matrices of elastic α - ^{12}C scattering at low energies in effective field theory

Shung-Ichi Ando¹,

*Department of Display and Semiconductor Engineering,
Sunmoon University, Asan, Chungnam 31460, Republic of Korea*

The elastic α - ^{12}C scattering at low energies for $l = 0, 1, 2, 3, 4, 5, 6$ is studied in effective field theory. We discuss the construction of the S matrices of elastic α - ^{12}C scattering in terms of the amplitudes of sub-threshold bound and resonant states of ^{16}O , which are calculated from the effective Lagrangian. The parameters appearing in the S matrices are fitted to the phase shift data below the p - ^{15}N breakup threshold energy, and we find that the phase shifts are well described within the theory.

PACS(s): 11.10.Ef, 24.10.-i, 25.55.-e, 26.20.Fj

¹mailto:sando@sunmoon.ac.kr

1. Introduction

Radiative α capture on carbon-12, $^{12}\text{C}(\alpha, \gamma)^{16}\text{O}$, is a fundamental reaction in nuclear astrophysics, which determines the C/O ratio along with the triple- α process in the helium burning process in stars [1]. The radiative capture rate at the Gamow peak energy, $E_G = 0.3$ MeV, in the stars is, however, difficult to measure in the experimental facilities because of the Coulomb barrier. One needs to employ a theoretical model, fit the parameters of the model to the experimental data measured at a few MeV energy or larger, and extrapolate the reaction rate down to the Gamow peak energy, $E_G = 0.3$ MeV. Over the last half-century, many experimental and theoretical studies have been carried out. See, e.g., Refs. [2, 3, 4, 5, 6, 7] for review.

The experimental data of elastic α - ^{12}C scattering provide us important information about the energies and widths of resonant states of ^{16}O at low energies, which are used to fix some parameters of theoretical models. The first integrated phase shift analysis of the elastic scattering for $l = 0, 1, 2, 3, 4, 5, 6$ was reported with the data taken at the Ruhr-Universität Bochum by Plaga et al in 1987 [8]. The upgraded precise phase shift analysis for partial waves, $l = 0, 1, 2, 3, 4, 5, 6$, was reported with the data taken at the University of Notre Dame by Tischhauser et al. in 2009 [9] where the energy range of the α particle is $2.6 \text{ MeV} \leq E_\alpha \leq 6.62 \text{ MeV}$; E_α is the α energy in the lab frame. In this work, we study the elastic α - ^{12}C scattering at low energies by employing an effective field theory (EFT).

To construct an EFT, one first needs to introduce a large momentum scale, Λ_H . An EFT is constructed by using the relevant degrees of freedom at low energy, below the large momentum scale, Λ_H . Then, the theory provides us a perturbative (derivative) expansion scheme in powers of Q/Λ_H where Q is a typical momentum scale in a reaction in question. The coefficients of effective Lagrangian are fixed by using experimental data, though they, in principle, can be determined from its mother theory [10]. An EFT is constructed for few-body nuclear systems, known as pionless EFT, in which the pions are regarded as irrelevant degrees of freedom, and one has $\Lambda_H = m_\pi$ where m_π is the pion mass [11]. In addition, the dibaryon fields which have the baryon number, $B = 2$, are introduced in the theory to expand the terms around the unitary limit [12, 13, 14]. This expansion scheme turns out to reproduce the effective range expansion [15]. Furthermore, one can naturally extend the formalism to the studies of reactions involving photo emission [16, 17, 18], β emission [19, 20, 21], and neutrino reactions [22, 23]. In the previous studies, we constructed an EFT for the $^{12}\text{C}(\alpha, \gamma)^{16}\text{O}$ reaction at the Gamow-peak energy, $E_G = 0.3$ MeV, and studied the elastic α - ^{12}C scattering at low energies for $l = 0, 1, 2, 3$ with and without the sub-threshold bound states of ^{16}O [24, 25]. We subsequently studied the $E1$ transition of the $^{12}\text{C}(\alpha, \gamma)^{16}\text{O}$ reaction [26] and the β -delayed α -emission from ^{16}N [7] in the EFT.

The inclusion of a resonant state in EFT has been studied by many authors, e.g., by Gelman [27] and by Habashi, Fleming, and van Kolck [28]; one needs to sum the leading order interactions up to the infinite order at the vicinity of resonant energy, where in most cases ones consider a resonant state and a background contribution. In real situations, on the other hand, a number of resonant states are involved. In the previous work, we

studied the elastic α - ^{12}C scattering for $l = 2$ including the sub-threshold 2_1^+ state and two resonant 2_2^+ and 2_3^+ states of ^{16}O , in which the S matrix is constructed from the amplitudes of those sub-threshold and resonant states; the amplitudes are derived from the effective Lagrangian and represented in terms of the effective range parameters [29]. In the present work, we apply the method to the study of the elastic α - ^{12}C scattering at low energies for $l = 0, 1, 2, 3, 4, 5, 6$. The parameters in the S matrices are fitted to the phase shift data below the p - ^{15}N breakup threshold energy, and we find that the phase shifts are well described within the theory. Then, we discuss the implication of the result for the application of EFT to the study of nuclear reactions in stellar evolution.

The present work is organized as the following. In section 2, an expression of the S matrices is introduced and the effective Lagrangian is presented, and, in section 3, the elastic scattering amplitudes of the sub-threshold and resonant states for the l -th partial wave states are derived from the Lagrangian. In section 4, we discuss the numerical results of the parameter fit to the phase shift data for $l = 0, 1, 2, 3, 4, 5, 6$, and finally in section 5, the results and discussion of this work are presented.

2. S matrices and effective Lagrangian

The construction of the S matrix of the elastic α - ^{12}C scattering for $l = 2$ was discussed in Ref. [29]. In this section, we review the method to extend it to the cases for l -th partial wave states. The S matrices of the elastic α - ^{12}C scattering for l -th partial wave channels are given as

$$S_l = e^{2i\delta_l}, \quad (1)$$

where δ_l is the phase shift of elastic scattering for l -th partial wave channel whose experimental data for $l = 0, 1, 2, 3, 4, 5, 6$ at $2.6 \text{ MeV} \leq E_\alpha \leq 6.62 \text{ MeV}$ are reported by Tischhauser et al. [9].² The scattering amplitude \tilde{A}_l is related to the S matrix as³

$$S_l = 1 + 2ip\tilde{A}_l. \quad (2)$$

Various resonant states of ^{16}O appear in the phase shift data, and the sub-threshold bound states and resonant states at high energy (above the maximum energy of the data) may give contributions to the S matrices of elastic α - ^{12}C scattering. In Table 1, we present a list of the sub-threshold bound states, the resonant states appearing in the phase shift data, and the resonant states as background contributions from high energy for the partial wave states of α - ^{12}C system. By employing those states in the table, we construct the S matrices of the elastic α - ^{12}C scattering.

To construct an S matrix, S_l , we may decompose a phase shift δ_l , for example, in the case of a sub-threshold bound state and two resonant states, as [27]

$$\delta_l = \delta_l^{(bs)} + \delta_l^{(rs1)} + \delta_l^{(rs2)}, \quad (3)$$

²The α energy labeled by E_α is in the lab frame, and the other energies are given in the center-of-mass frame.

³There is a common factor difference between the expression of the amplitude \tilde{A}_l and the standard form of the amplitude A_l ; $A_l = \frac{2\pi}{\mu}(2l+1)e^{2i\sigma_l}\tilde{A}_l$ where σ_l is the Coulomb phase shift for l , $e^{2i\sigma_l} = \Gamma(l+1+i\eta)/\Gamma(l+1-i\eta)$ with $\eta = \kappa/p$.

l	(Bound states)	$2.6 \text{ MeV} \leq E_\alpha \leq 6.62 \text{ MeV}$,	$6.62 \text{ MeV} < E_\alpha$
0	0_2^+	0_3^+	0_4^+
1	1_1^-	1_2^-	1_3^-
2	2_1^+	$2_2^+, 2_3^+$	2_4^+
3	3_1^-	3_2^-	3_3^-
4	—	$4_1^+, 4_2^+$	4_3^+
5	—	—	5_1^-
6	(bg)	—	6_1^+

Table 1: Bound and resonant (l_{i-th}^π) states of ^{16}O , which are used to construct the S matrices for l -th partial wave states of elastic α - ^{12}C scattering; the resonant states in the second column appear in the energy range, $2.6 \text{ MeV} \leq E_\alpha \leq 6.62 \text{ MeV}$, and those in the third column do at $6.62 \text{ MeV} < E_\alpha$.

where $\delta_l^{(bs)}$ is a phase shift from a sub-threshold bound state, and $\delta_2^{(rsN)}$ with $N = 1, 2$ are those from resonant states. We now assume that each of those phase shifts may have a relation to a corresponding scattering amplitude as

$$e^{2i\delta_l^{(ch)}} = 1 + 2ip\tilde{A}_l^{(ch)}, \quad (4)$$

where $ch(annel) = bs, rs1, rs2$, and $\tilde{A}_l^{(bs)}$ and $\tilde{A}_l^{(rsN)}$ with $N = 1, 2$ are the amplitudes for the binding part and the first and second resonant parts of the amplitudes, which will be constructed from the effective Lagrangian in the next section. Thus, the total amplitude \tilde{A}_l for the nuclear reaction part in terms of the three amplitudes, $\tilde{A}_l^{(bs)}$ and $\tilde{A}_l^{(rsN)}$ with $N = 1, 2$, is

$$\tilde{A}_l = \tilde{A}_l^{(bs)} + e^{2i\delta_l^{(bs)}}\tilde{A}_l^{(rs1)} + e^{2i(\delta_l^{(bs)} + \delta_l^{(rs1)})}\tilde{A}_l^{(rs2)}. \quad (5)$$

We note that the total amplitudes, \tilde{A}_l , are not obtained as the summation of the amplitudes, $\tilde{A}_l^{(bs)}$ and $\tilde{A}_l^{(rsN)}$ with $N = 1, 2$, but have the additional phase factors to $\tilde{A}_l^{(rsN)}$ with $N = 1, 2$, and the order of the three amplitudes, $\tilde{A}_l^{(bs)}$ and $\tilde{A}_l^{(rsN)}$ with $N = 1, 2$ are exchangeable.

To study the elastic α - ^{12}C scattering at low energies in EFT, we choose the p - ^{15}N breakup threshold energy as the high energy scale. For the relevant degrees of freedom of the theory, the ground 0^+ states of α and ^{12}C are chosen as elementary-like scalar fields. We also introduce the composite fields of α and ^{12}C to describe the sub-threshold and resonant states of ^{16}O . An effective Lagrangian to derive the scattering amplitude for the l -th wave elastic α - ^{12}C scattering at low energies including l_{i-th}^π states of ^{16}O may be written as [24, 25]

$$\mathcal{L} = \phi_\alpha^\dagger \left(iD_0 + \frac{\vec{D}^2}{2m_\alpha} \right) \phi_\alpha + \phi_C^\dagger \left(iD_0 + \frac{\vec{D}^2}{2m_C} \right) \phi_C$$

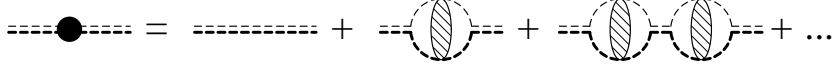


Figure 1: Diagrams for dressed ^{16}O propagator. A thick (thin) dashed line represents a propagator of ^{12}C (α), and a thick and thin double dashed line with and without a filled circle represent a dressed and bare ^{16}O propagator, respectively. A shaded blob represents a set of diagrams consisting of all possible one-potential-photon-exchange diagrams up to infinite order and no potential-photon-exchange one.

$$\begin{aligned}
& + \sum_{l=0}^6 \sum_i \sum_{k=0}^3 C_{(li)k} d_{(li)}^\dagger \left[iD_0 + \frac{\vec{D}^2}{2(m_\alpha + m_C)} \right]^k d_{(li)} \\
& - \sum_{l=0}^6 \sum_i y_{(li)} \left[d_{(nr)}^\dagger (\phi_\alpha O_{(l)} \phi_C) + (\phi_\alpha O_{(l)} \phi_C)^\dagger d_{(li)} \right], \tag{6}
\end{aligned}$$

where ϕ_α (m_α) and ϕ_C (m_C) are scalar fields (masses) of α and ^{12}C , respectively. D^μ is a covariant derivative, $D^\mu = \partial^\mu + i\mathcal{Q}A^\mu$ where \mathcal{Q} is a charge operator and A^μ is the photon field. $d_{(li)}$ are the composite fields for the l_{i-th}^π states of ^{16}O consisting of α and ^{12}C fields in l -th partial wave states, which are introduced for perturbative expansion around the unitary limit [12, 13, 14, 15]. The field $d_{(li)}$ are tensors in general, which are represented as Cartesian tensors of rank l [30, 31, 32] (we suppressed the indices of the Cartesian tensors); $O_{(l)}$ are also tensors to project the α - ^{12}C system to l -th partial wave states. The coupling constants, $C_{(li)k}$ with $k = 0, 1, 2, 3$, correspond to the effective range parameters of elastic α - ^{12}C scattering; for those of the sub-threshold states of ^{16}O , the first coupling constants, $C_{(li)k}$ with $k = 0$, are fixed by using the binding energies of the sub-threshold states and the other parameters are fitted to the experimental phase shift data with other parameters appearing in the S matrices. For the coupling constants of the resonant parts, $C_{(li)k}$ with $k = 0, 1, 2, 3$, the first two terms, $C_{(li)k}$ with $k = 0, 1$, are rewritten by using the resonant energies and widths of the resonant states of ^{16}O , respectively. The third and fourth parameters for the resonant states, $C_{(li)k}$ with $k = 2, 3$ are fitted to the phase shift data. The coupling constants $y_{(li)}$ are convention-dependent [33], and we take the convenient choice; $y_{(li)} = \sqrt{2\pi(2l+1)\mu^{2l-1}}$ where μ is the reduced mass of α and ^{12}C .

3. Scattering amplitudes

All the scattering amplitudes, $\tilde{A}_l^{(bs)}$ and $\tilde{A}_l^{(rsN)}$ with $N = 1, 2, 3$, are calculated from the diagrams depicted in Figs. 1 and 2. The shaded blobs in the diagrams represent the parts of the non-perturbative Coulomb interaction, the Coulomb propagator in the one-loop diagrams and the Coulomb wavefunctions for the initial and final state interactions. Here, the bubble diagrams are summed up to infinite order in Fig. 1. For the bound parts of the amplitudes, we treat them non-perturbatively though they can be expanded perturbatively at the energy region of the experimental data. For the resonant parts of the amplitudes (for our case, they are classified as narrow resonances because of $\Gamma_r \ll E_r$ [28]),

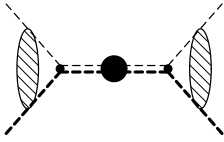


Figure 2: Diagram of the scattering amplitude. See the caption of Fig. 1 as well.

the counting rules of resonant states are carefully studied by Gelman [27] and Habashi, Fleming, and van Kolck [28]. The energy range of phase shift data covers the resonant states, and at the vicinities of the resonant energies we should have the amplitudes for which the bubble diagrams are summed up to the infinite order. While at the off-resonant energy regions, one can expand the resonant amplitudes perturbatively and the $d_{(li)}$ fields may start mixing through the bubble diagram for corrections at higher orders. We keep the summed amplitudes for the resonant states as leading contributions and ignore the field mixing.

For the bound state amplitudes, $\tilde{A}_l^{(bs)}$ with $l = 0, 1, 2, 3$, we have [24, 25]

$$\tilde{A}_l^{(bs)} = \frac{C_\eta^2 W_l(p)}{K_l(p) - 2\kappa H_l(p)}, \quad (7)$$

where the function $C_\eta^2 W_l(p)$ in the numerator of the amplitude is calculated from the initial and final state Coulomb interactions in Fig. 2; p is the magnitude of relative momentum of the $\alpha-{}^{12}\text{C}$ system in the center of mass frame, $p = \sqrt{2\mu E}$, and one has

$$C_\eta^2 = \frac{2\pi\eta}{\exp(2\pi\eta) - 1}, \quad (8)$$

$$W_l(p) = \left(\frac{\kappa^2}{l^2} + p^2 \right) W_{l-1}(p), \quad W_0(p) = 1, \quad (9)$$

where $\eta = \kappa/p$: κ is the inverse of the Bohr radius, $\kappa = Z_\alpha Z_{12C} \alpha_E \mu$, where Z_A is the number of protons of the nuclei, $Z_\alpha = 2$ and $Z_{12C} = 6$, and α_E is the fine structure constant. The function $-2\kappa H_l(p)$ in the denominator of the amplitude is the Coulomb self-energy term which is calculated from the loop diagram in Fig. 1, and one has

$$H_l(p) = W_l(p) H(\eta), \quad H(\eta) = \psi(i\eta) + \frac{1}{2i\eta} - \log(i\eta), \quad (10)$$

where $\psi(z)$ is the digamma function. The nuclear interaction is represented in terms of the effective range parameters in the function $K_l(p)$ in the denominator of the amplitude in Eq. (7). As discussed in Ref. [24], large and significant contributions to the series of effective range expansion, compared to that evaluated from the phase shift data at the lowest energy of the data, $E_\alpha = 2.6$ MeV, appear from the Coulomb self-energy term, $-2\kappa H_l(p)$. In order to subtract those contributions, we include the effective range terms

up to p^6 order for $l = 0, 1, 2$ and those up to p^8 order for $l = 3$ as counter terms. Thus, we have

$$K_l(p) = -\frac{1}{a_l} + \frac{1}{2}r_l p^2 - \frac{1}{4}P_l p^4 + Q_l p^6 - R_l p^8, \quad (11)$$

where a_l, r_l, P_l, Q_l, R_l are effective range parameters. (We note that $R_l = 0$ for $l = 0, 1, 2$.)

Now we fix a parameter among the five effective range parameters, a_l, r_l, P_l, Q_l , and R_l by using the condition that the inverse of the scattering amplitude $\tilde{A}_l^{(bs)}$ vanishes at the binding energy of the sub-threshold states of ^{16}O . Thus, the denominator of the scattering amplitude,

$$D_l(p) = K_l(p) - 2\kappa H_l(p), \quad (12)$$

vanishes at $p = i\gamma_l$ where γ_l are the binding momenta of the $0_2^+, 1_1^-, 2_1^+, 3_1^-$ (l_{i-th}^π) states of ^{16}O ; $\gamma_l = \sqrt{2\mu B_l}$ where B_l are the binding energies of the bound states of ^{16}O from the α - ^{12}C breakup threshold. At the binding energies, we have the wavefunction normalization factors $\sqrt{Z_l}$ for the bound states of ^{16}O in the dressed ^{16}O propagators as

$$\frac{1}{D_l(p)} = \frac{Z_l}{E + B_l} + \dots, \quad (13)$$

where the dots denote the finite terms at $E = -B_l$. Thus, one has

$$\sqrt{Z_l} = \left(\left| \frac{dD_l(p)}{dE} \right|_{E=-B_l} \right)^{-1/2} = \left(2\mu \left| \frac{dD_l(p)}{dp^2} \right|_{p^2=-\gamma_l^2} \right)^{-1/2}. \quad (14)$$

The wavefunction normalization factor $\sqrt{Z_l}$ is multiplied to a reaction amplitude when a bound state appears in the initial or final state of the reaction.

Using the condition, $D_l(i\gamma_l) = 0$, we fix the effective range parameter a_l as

$$-\frac{1}{a_l} = \frac{1}{2}\gamma_l^2 r_l + \frac{1}{4}\gamma_l^4 P_l + \gamma_l^6 Q_l + \gamma_l^8 R_l + 2\kappa H_l(i\gamma_l). \quad (15)$$

Using the relation of Eq. (15), we rewrite the denominator of the amplitude $D_l(p)$ as

$$D_l(p) = \frac{1}{2}r_l(\gamma_l^2 + p^2) + \frac{1}{4}P_l(\gamma_l^4 - p^4) + Q_l(\gamma_l^6 + p^6) + R_l(\gamma_l^8 - p^8) + 2\kappa [H_2(i\gamma_l) - H_l(p)], \quad (16)$$

where we have three constants, r_l, P_l, Q_l for $l = 0, 1, 2$ and four constants, r_3, P_3, Q_3, R_3 for $l = 3$ in the function $D_l(p)$ for the non-resonant amplitude $\tilde{A}_l^{(bs)}$, which are fitted to the phase shift data. For the study of the asymptotic normalization coefficients (ANC), the exponential factors in Eq. (5) almost become ones at the small energy region due to the Gamow factor in C_η^2 , and the amplitudes become

$$\tilde{A}_l = \tilde{A}_l^{(bs)} + \tilde{A}_l^{(rs1)} + \tilde{A}_l^{(rs2)} + O(C_\eta^4), \quad (17)$$

where the poles at the sub-threshold bound states of ^{16}O exist in $\tilde{A}_l^{(bs)}$, the ANC s $|C_b|$ for the sub-threshold bound states of ^{16}O are calculated by using the formula [34]

$$|C_b| = \frac{\gamma_l^l}{l!} \Gamma(l+1 + \kappa/\gamma_l) \left(\left| \frac{dD_l(p)}{dp^2} \right|_{p^2=-\gamma_l^2} \right)^{-1/2} (\text{fm}^{-1/2}), \quad (18)$$

where $\Gamma(x)$ is the gamma function, and one may notice that the ANC s are proportional to the wavefunction normalization factor $\sqrt{Z_l}$. We note that the ANC s themselves are not necessary for the calculations of EFT (while they may become constraints when the experimental data are not available for fitting the effective range parameters). In the present work, we display the values of the ANC s (in the next section) as a demonstration of the comparison with those obtained in our previous works as well as the other theoretical models. In addition, we perform a test calculation to study the values of ANC s from a potential model. Its results are presented in the appendix.

For the elastic scattering amplitudes for the resonant states of ^{16}O , we may first have those amplitudes as the same expression of the bound state amplitudes in Eq. (7) in terms of the effective range parameters as

$$\tilde{A}_l^{(rsN)} = \frac{C_\eta^2 W_l(p)}{K_l^{(rsN)}(p) - 2\kappa H_l(p)}, \quad (19)$$

with $N = 1, 2, 3$, which correspond to the first, second, and third resonant states of ^{16}O , respectively, for l -th partial wave states and

$$K_l^{(rsN)}(p) = -\frac{1}{a_l^{(rsN)}} + \frac{1}{2} r_l^{(rsN)} p^2 - \frac{1}{4} P_l^{(rsN)} p^4 + Q_l^{(rsN)} p^6, \quad (20)$$

where we include the terms up to p^6 order for all the resonant amplitudes.

We now introduce the Taylor expansion around the resonant energies in the denominator of the scattering amplitudes [35]. Thus, we rewrite the amplitudes as

$$\tilde{A}_l^{(rsN)} = -\frac{1}{p} \frac{\frac{1}{2} \Gamma_{(li)}(E)}{E - E_{R(li)} + R_{(li)}(E) + i \frac{1}{2} \Gamma_{(li)}(E)}, \quad (21)$$

with

$$\Gamma_{(li)}(E) = \Gamma_{R(li)} \frac{p C_\eta^2 W_l(p)}{p_r C_{\eta_r}^2 W_l(p_r)}, \quad (22)$$

$$R_{(li)}(E) = a_{(li)}(E - E_{R(li)})^2 + b_{(li)}(E - E_{R(li)})^3, \quad (23)$$

where

$$a_{(li)} = \frac{1}{2} Z_{R(li)} \left(2P_l^{(rsN)} \mu^2 - 48Q_l^{(rsN)} \mu^3 E_{R(li)} + 2\kappa \text{Re} \left. \frac{\partial^2 H_l}{\partial E^2} \right|_{E=E_{R(li)}} \right), \quad (24)$$

$$b_{(li)} = \frac{1}{6} Z_{R(li)} \left(-48Q_l^{(rsN)} \mu^3 + 2\kappa \operatorname{Re} \frac{\partial^3 H_l}{\partial E^3} \Big|_{E=E_{R(li)}} \right), \quad (25)$$

$$Z_{R(li)}^{-1} = \operatorname{Re} \frac{\partial}{\partial E} D_l^{(rsN)}(E) \Big|_{E=E_{R(li)}}, \quad Z_{R(li)} = \frac{\Gamma_{R(li)}}{2p_r W_l(p_r) C_{\eta_r}^2}. \quad (26)$$

In the above equations, $E_{R(li)}$ and $\Gamma_{R(li)}$ are the energies and the widths of the resonant l_{i-th}^π states of ^{16}O , and p_r are the resonant momenta, $p_r = \sqrt{2\mu E_{R(li)}}$, which also appear in η_r as $\eta_r = \kappa/p_r$. We note that the expression of Eq. (21) resembles that of the Breit-Wigner formula, but it is derived from the expression of the effective range expansion in Eq. (20); it has the additional terms, the corrections of the higher order terms being proportional to $(E - E_{R(li)})^2$ and $(E - E_{R(li)})^3$ in the function $R_{(li)}(E)$ in Eq. (23); though the coefficients $a_{(li)}$ and $b_{(li)}$ are functions of the effective range parameters, $P_l^{(rsN)}$ and $Q_l^{(rsN)}$, we treat $a_{(li)}$ and $b_{(li)}$ as independent free parameters for the sake of simplicity.

Using the expression of the amplitudes in Eqs. (7) and (21), we obtain an expression of the S matrices in Eq. (1) as

$$e^{2i\delta_l} = \frac{K_l(p) - 2\kappa \operatorname{Re} H_l(p) + ip C_\eta^2 W_l(p)}{K_l(p) - 2\kappa \operatorname{Re} H_l(p) - ip C_\eta^2 W_l(p)} \prod_i \frac{E - E_{R(li)} + R_{(li)}(E) - i\frac{1}{2}\Gamma_{(li)}(E)}{E - E_{R(li)} + R_{(li)}(E) + i\frac{1}{2}\Gamma_{(li)}(E)}, \quad (27)$$

where the part for the bound states in terms of $K_l(p) - 2\kappa \operatorname{Re} H_l(p) \pm ip C_\eta^2 W_l(p)$ appear for $l = 0, 1, 2, 3$, and we also include it for $l = 6$ as a background contribution from low energy. The part of the resonant states in terms of $E - E_{R(li)} + R_{(li)}(E) \mp i\frac{1}{2}\Gamma_{(li)}(E)$ are for those appearing in the energy range of the phase shift data, and we also include it for each of the partial waves as a background contribution from high energy.

4. Numerical results

We construct an S matrix of the elastic scattering for each of the partial waves, $l = 0, 1, 2, 3, 4, 5, 6$, and fit parameters in the S matrices to the phase shift data at $2.6 \text{ MeV} < E_\alpha < 6.62 \text{ MeV}$ reported by Tischhauser et al. [9], by means of a Markov chain Monte Carlo (MCMC) program [36]. We will see that curves calculated by using the fitted parameters reproduce the phase shift data very well.

4.1 Phase shift for $l = 0$ channel

We consider three states, 0_2^+ , 0_3^+ , 0_4^+ states of ^{16}O for the S matrix of elastic α - ^{12}C scattering for $l = 0$, where 0_2^+ is the sub-threshold bound state, 0_3^+ is the resonant state appearing in the phase shift data at $E_\alpha = 6.52 \text{ MeV}$, and 0_4^+ is the resonant state as a background contribution from high energy appearing at $E_\alpha = 9.16 \text{ MeV}$. Thus, we have an expression of the S matrix for $l = 0$ as

$$e^{2i\delta_0} = \frac{K_0(p) - 2\kappa \operatorname{Re} H_0(p) + ip C_\eta^2}{K_0(p) - 2\kappa \operatorname{Re} H_0(p) - ip C_\eta^2} \prod_{i=3}^4 \frac{E - E_{R(0i)} + R_{(0i)}(E) - i\frac{1}{2}\Gamma_{(0i)}(E)}{E - E_{R(0i)} + R_{(0i)}(E) + i\frac{1}{2}\Gamma_{(0i)}(E)}, \quad (28)$$

with

$$K_0(p) = \frac{1}{2} r_0 (\gamma_0^2 + p^2) + \frac{1}{4} P_0 (\gamma_0^4 - p^4) + Q_0 (\gamma_0^6 + p^6) + 2\kappa H_0(i\gamma_0), \quad (29)$$

$$\Gamma_{(0i)}(E) = \Gamma_{R(0i)} \frac{p C_\eta^2 W_0(p)}{p_r C_{\eta_r}^2 W_0(p_r)}, \quad (30)$$

$$R_{(0i)}(E) = a_{(0i)}(E - E_{R(0i)})^2 + b_{(0i)}(E - E_{R(0i)})^3, \quad i = 3, 4 \quad (31)$$

where $\gamma_0 = \sqrt{2\mu B_0}$ and $p_r = \sqrt{2\mu E_{(0i)}}$. Thus, we have 7 parameters to fit the data,

$$\theta_0 = \{r_0, P_0, Q_0, E_{R(03)}, \Gamma_{R(03)}, a_{(04)}, b_{(04)}\}, \quad (32)$$

where two parameters $a_{(03)}$ and $b_{(03)}$ are set to be zero, $a_{(03)} = b_{(03)} = 0$, because they are not sensitive to the parameter fit. We use the experimental values for $E_{R(04)}$ and $\Gamma_{R(04)}$, $E_{R(04)}^{(exp)} = 6.870(15)$ MeV and $\Gamma_{R(04)}^{(exp)} = 185(35)$ keV [37], because they are not covered by the phase shift data, to which one cannot fit them.

In Table 2, we show fitted values and their errors of the 7 parameters in the amplitudes of the 0_2^+ , 0_3^+ , 0_4^+ states of ^{16}O in the S matrix of elastic α - ^{12}C scattering for $l = 0$ in Eq. (28) where we find a small value of χ^2/N , $\chi^2/N = 0.013$, for the parameter fit, as shown in Table 3. The fitted values of $E_{R(03)}$ and $\Gamma_{R(03)}$ agree with their experimental values, $E_{R(03)}^{(exp)} = 4.887(2)$ MeV and $\Gamma_{R(03)}^{(exp)} = 1.5(5)$ keV [37]. Those of the parameters, such as P_0 , $a_{(03)}$, and $b_{(03)}$, at higher order have large errors. One may notice that the errors of the effective range parameters, r_0 , P_0 , Q_0 become larger in order as the orders of the p^2 expansion increase. This may indicate that the perturbative expansion in the effective range parameters works well.

In Table 4, we show a value of the ANC, $|C_b|$, of the 0_2^+ state of ^{16}O ; we obtain $|C_b| = 370(25)$ fm $^{-1/2}$, which is smaller than our previous estimates, $|C_b| = 443(3)$ fm $^{-1/2}$ [24] and $|C_b| = (6.4\text{--}7.4) \times 10^2$ fm $^{-1/2}$ [38]. We note that the values of ANC of the 0_2^+ state of ^{16}O reported in the literature are still scattered: from the R -matrix analysis, the reported values of ANC are $|C_b| = 44^{+270}_{-40}$ fm $^{-1/2}$ [39], 1800 fm $^{-1/2}$ [40], and 1560 fm $^{-1/2}$ [5], from the α transfer reaction, 1560(100) fm $^{-1/2}$ [41], and from those fitting the phase shift data using the square-well potential, 3218.46 fm $^{-1/2}$ [42] and 886 – 1139 fm $^{-1/2}$ [43], and using the so-called Δ -method, 406 fm $^{-1/2}$ [44] and 293 fm $^{-1/2}$ [45]. So, this would be an interesting issue to investigate in the future.

In Fig. 3, we plot a curve of the phase shift for $l = 0$, δ_0 , by using the fitted values of the parameters obtained in Table 2. The phase shift data are also displayed in the figure. We find that the fitted curve agrees well with the phase shift data.

4.2 Phase shift for $l = 1$ channel

We consider three states, 1_1^- , 1_2^- , 1_3^- states of ^{16}O to construct the S matrix of elastic α - ^{12}C scattering for $l = 1$ where 1_1^- is the sub-threshold bound state, 1_2^- is the resonant state appearing in the phase shift data at $E_\alpha = 3.23$ MeV, and 1_3^- is a resonant state as a background contribution from high energy appearing at $E_\alpha = 7.04$ MeV. Because the resonant 1_2^- state can be described by the effective range parameters for the sub-threshold bound 1_1^- state, as discussed in Ref. [26], we include the 1_2^- state in the amplitude of the sub-threshold 1_1^- state. Thus, we have an expression of the S matrix for $l = 1$ as

$$e^{2i\delta_1} = \frac{K_1(p) - 2\kappa Re H_1(p) + ip C_\eta^2 W_1(p)}{K_1(p) - 2\kappa Re H_1(p) - ip C_\eta^2 W_1(p)} \frac{E - E_{R(13)} + R_{(13)}(E) - i\frac{1}{2}\Gamma_{(13)}(E)}{E - E_{R(13)} + R_{(13)}(E) + i\frac{1}{2}\Gamma_{(13)}(E)}, \quad (33)$$

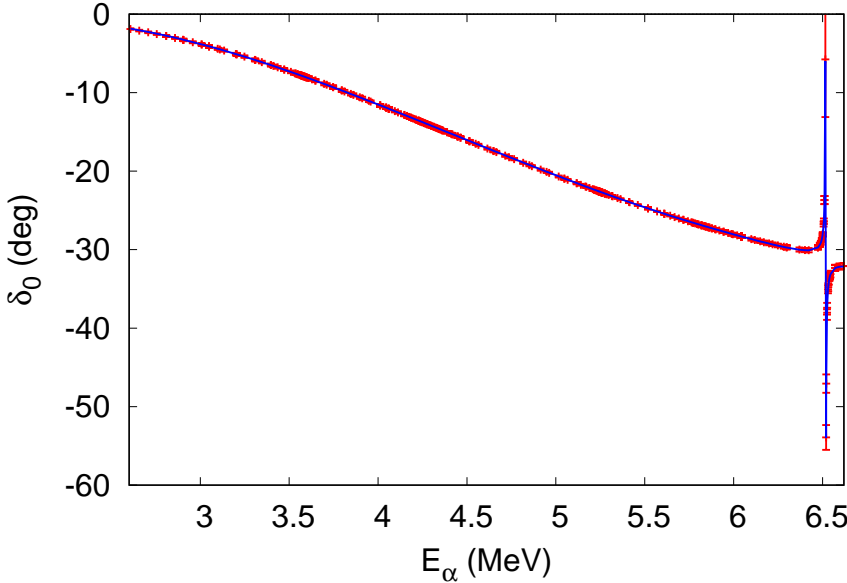


Figure 3: Phase shift δ_0 of elastic α - ^{12}C scattering for s -wave channel as a function of E_α calculated by using the fitted values of the parameters. Experimental data are included in the figure as well.

with

$$K_1(p) = \frac{1}{2}r_1(\gamma_1^2 + p^2) + \frac{1}{4}P_1(\gamma_1^4 - p^4) + Q_1(\gamma_1^6 + p^6) + 2\kappa H_1(i\gamma_1), \quad (34)$$

$$\Gamma_{(13)}(E) = \Gamma_{R(13)} \frac{p C_\eta^2 W_1(p)}{p_r C_{\eta_r}^2 W_1(p_r)}, \quad (35)$$

$$R_{(13)}(E) = a_{(13)}(E - E_{R(13)})^2 + b_{(13)}(E - E_{R(13)})^3, \quad (36)$$

where $\gamma_1 = \sqrt{2\mu B_1}$ and $p_r = \sqrt{2\mu E_{R(13)}}$. We have 5 parameters to fit the data as

$$\theta_1 = \{r_1, P_1, Q_1, a_{(13)}, b_{(13)}\}, \quad (37)$$

and we use the experimental values for $E_{R(13)}$ and $\Gamma_{R(13)}$, $E_{R(13)}^{(exp)} = 5.278(2)$ MeV and $\Gamma_{R(13)}^{(exp)} = 91(6)$ keV [37], for the background contribution from high energy.

In Table 2, we show fitted values and their errors of the 5 parameters in the amplitudes of the 1_1^- , 1_2^- , 1_3^- states of ^{16}O in the S matrix of elastic α - ^{12}C scattering for $l = 1$ in Eq. (33) where we find a small value of χ^2/N , $\chi^2/N = 0.089$, for the parameter fit, as shown in Table 3. We also find relatively large error bars of the coefficients $a_{(13)}$ and $b_{(13)}$ at the high order while all errors of the effective range coefficients, r_1 , P_1 , Q_1 , turn out to be small presumably because those parameters need to fit the resonant 1_2^- state of

^{16}O appearing in the phase shift data. In Table 4, we show the value of the ANC of the sub-threshold 1_1^- state of ^{16}O ; we have $|C_b| = 1.727(3) \times 10^{14} \text{ fm}^{-1/2}$ which agrees well to our previous estimate, $|C_b| = (1.6\text{--}1.9) \times 10^{14} \text{ fm}^{-1/2}$ [24]. In Fig. 4, we plot a curve

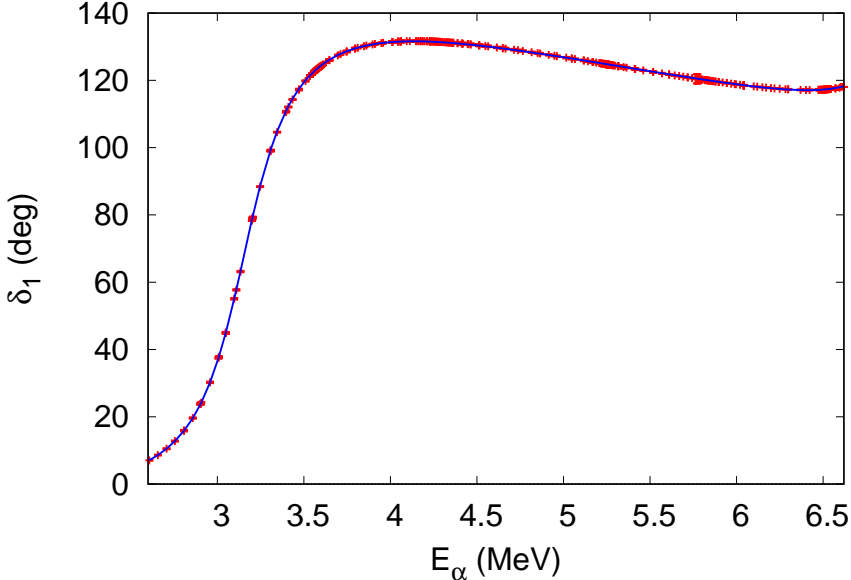


Figure 4: Phase shift δ_1 of elastic α - ^{12}C scattering for p -wave channel as a function of E_α calculated by using the fitted values of the parameters. Experimental data are included in the figure as well.

of the phase shift for $l = 1$, δ_1 , by using the fitted values of the parameters obtained in Table 2. The phase shift data are also displayed in the figure. We find that the fitted curve agrees well with the phase shift data. As discussed in Ref. [26], the phase shift data up to $E_\alpha = 6$ MeV can be described by the three effective range parameters only, and the tail of the phase shift data at the high-energy side is now described by the background contribution of the resonant 1_3^- state of ^{16}O from high energy.

4.3 Phase shift for $l = 2$ channel

We include the 2_1^+ , 2_2^+ , 2_3^+ , 2_4^+ states of ^{16}O to construct an S matrix for $l = 2$ where 2_1^+ is the sub-threshold bound state, 2_2^+ and 2_3^+ are the resonant states appearing in the phase shift data at $E_\alpha = 3.58$ MeV and $E_\alpha = 5.81$ MeV, respectively, and 2_4^+ is a resonant state as a background contribution from high energy appearing at $E_\alpha = 7.81$ MeV. Thus, we have an expression of the S matrix for $l = 2$ as

$$e^{2i\delta_2} = \frac{K_2(p) + 2\kappa \text{Re}H_2(p) + ipC_\eta^2 W_2(p)}{K_2(p) + 2\kappa \text{Re}H_2(p) - ipC_\eta^2 W_2(p)}$$

$$\times \prod_{i=2}^4 \frac{E - E_{R(2i)} + R_{(2i)}(E) - i\frac{1}{2}\Gamma_{(2i)}(E)}{E - E_{R(2i)} + R_{(2i)}(E) + i\frac{1}{2}\Gamma_{(2i)}(E)}, \quad (38)$$

with

$$K_2(p) = \frac{1}{2}r_2(\gamma_2^2 + p^2) + \frac{1}{4}P_2(\gamma_2^4 - p^4) + Q_2(\gamma_2^6 + p^6) + 2\kappa H_2(i\gamma_0), \quad (39)$$

$$\Gamma_{(2i)}(E) = \Gamma_{R(2i)} \frac{p C_\eta^2 W_2(p)}{p_r C_{\eta_r}^2 W_2(p_r)}, \quad (40)$$

$$R_{(2i)}(E) = a_{(2i)}(E - E_{R(2i)})^2 + b_{(2i)}(E - E_{R(2i)})^3, \quad i = 2, 3, 4 \quad (41)$$

where $\gamma_2 = \sqrt{2\mu B_2}$ and $p_r = \sqrt{2\mu E_{(2i)}}$. We have 9 parameters to fit the data as

$$\theta_2 = \{r_2, P_2, Q_2, E_{R(22)}, \Gamma_{R(22)}, E_{R(23)}, \Gamma_{R(23)}, a_{(23)}, b_{(23)}\}, \quad (42)$$

where four parameters, $a_{(22)}$, $b_{(22)}$, $a_{(24)}$, $b_{(24)}$, are set to be zero, $a_{(22)} = b_{(22)} = a_{(24)} = b_{(24)} = 0$, because they are not sensitive to the parameter fit while we use the experimental values for $E_{R(24)}$ and $\Gamma_{R(24)}$, $E_{R(24)}^{(exp)} = 5.858(10)$ MeV and $\Gamma_{R(24)}^{(exp)} = 150(10)$ keV [37], for the background contribution from high energy.

In Table 2, we show fitted values and their errors of the 9 parameters in the amplitudes of the 2_1^+ , 2_2^+ , 2_3^+ , 2_4^+ states of ^{16}O in the S matrix of elastic α - ^{12}C scattering for $l = 2$ in Eq. (38) where we find a small value of χ^2/N , $\chi^2/N = 0.66$, for the parameter fit, as shown in Table 3. (Those values in the table are taken from Table 2 in Ref. [29].) The fitted values of $E_{R(22)}$, $\Gamma_{R(22)}$, $E_{R(23)}$, and $\Gamma_{R(23)}$ agree with their experimental values, $E_{R(22)}^{(exp)} = 2.68255(50)$ MeV, $\Gamma_{R(22)}^{(exp)} = 0.625(100)$ keV, $E_{R(23)}^{(exp)} = 4.358(4)$ MeV, $\Gamma_{R(23)}^{(exp)} = 71(3)$ keV [37] while the fitted values of the parameters, such as Q_2 , $a_{(23)}$, and $b_{(23)}$, at higher order have large errors. In Table 4, we show the value of the ANC of the sub-threshold 2_1^+ state of ^{16}O ; we have $|C_b| = 3.1(6) \times 10^4 \text{ fm}^{-1/2}$, which is larger than our previous estimate, $|C_b| = (2.1\text{--}2.4) \times 10^4 \text{ fm}^{-1/2}$ [24]. In addition, we also argued that the value of the ANC of the 2_1^+ state of ^{16}O is sensitive to conditions imposed on the effective range parameters, r_2 , P_2 , Q_2 , at very low energy region, $0 \leq E_\alpha \leq 2.6$ MeV, where no phase shift data are reported; we can even reproduce the large ANC value, $|C_b| \simeq 10 \times 10^4 \text{ fm}^{-1/2}$ reported from the α transfer experiments [46, 47, 48, 41]. For more details, refer to Ref. [29]. In Fig. 5, we plot a curve of the phase shift for $l = 2$, δ_2 , by using the fitted values of the parameters obtained in Table 2. The phase shift data are also displayed in the figure. We find that the fitted curve agrees well with the phase shift data.

4.4 Phase shift for $l = 3$ channel

We consider 3_1^- , 3_2^- , 3_3^- states of ^{16}O to construct an S matrix of elastic α - ^{12}C scattering for $l = 3$ where 3_1^- is the sub-threshold bound state, 3_2^- is the resonant state appearing in the phase shift data at $E_\alpha = 5.92$ MeV and 3_3^- is a resonant state as a background contribution from high energy appearing at $E_\alpha = 7.96$ MeV. Because the resonant 3_2^- state can be described by the effective range parameters as well, as we have seen in the

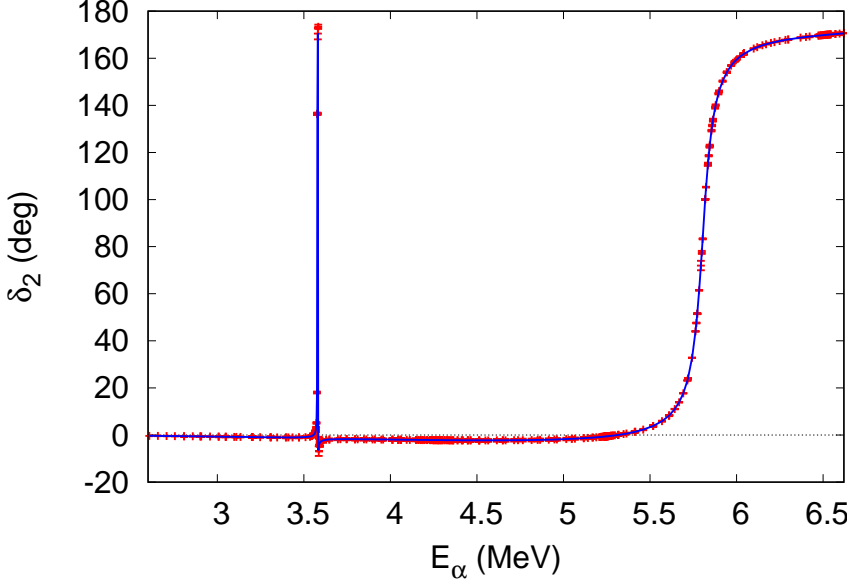


Figure 5: Phase shift δ_2 of elastic α - ^{12}C scattering for d -wave channel as a function of E_α calculated by using the fitted values of the parameters. Experimental data are included in the figure as well.

case of $l = 1$, we include the 3_2^- state in the amplitude of the sub-threshold 3_1^- state. Thus, we have an expression of the S matrix for $l = 3$ as

$$e^{2i\delta_3} = \frac{K_3(p) - 2\kappa \text{Re}H_3(p) + ipC_\eta^2W_3(p)}{K_3(p) - 2\kappa \text{Re}H_3(p) - ipC_\eta^2W_3(p)} \frac{E - E_{R(33)} + R_{(33)}(E) - i\frac{1}{2}\Gamma_{(33)}(E)}{E - E_{R(33)} + R_{(33)}(E) + i\frac{1}{2}\Gamma_{(33)}(E)}, \quad (43)$$

with

$$\begin{aligned} K_3(p) &= \frac{1}{2}r_3(\gamma_3^2 + p^2) + \frac{1}{4}P_3(\gamma_3^4 - p^4) + Q_3(\gamma_3^6 + p^6) + R_3(\gamma_3^8 - p^8) \\ &\quad + 2\kappa H_3(i\gamma_3), \end{aligned} \quad (44)$$

$$\Gamma_{(33)}(E) = \Gamma_{R(33)} \frac{pC_\eta^2W_3(p)}{p_r C_{\eta_r}^2 W_3(p_r)}, \quad (45)$$

$$R_{(33)}(E) = a_{(33)}(E - E_{R(33)})^2 + b_{(33)}(E - E_{R(33)})^3, \quad (46)$$

where $\gamma_3 = \sqrt{2\mu B_3}$ and $p_r = \sqrt{2\mu E_{R(33)}}$. We have 6 parameters to fit the data as

$$\theta_3 = \{r_3, P_3, Q_3, R_3, a_{(33)}, b_{(33)}\}, \quad (47)$$

where we impose a condition to the parameter R_3 for the parameter fit, $\tilde{R}_3 < R_3$; \tilde{R}_3 is the contribution from the Coulomb self-energy term, $-2\kappa H_3(p)$, to the R_3 term, and we

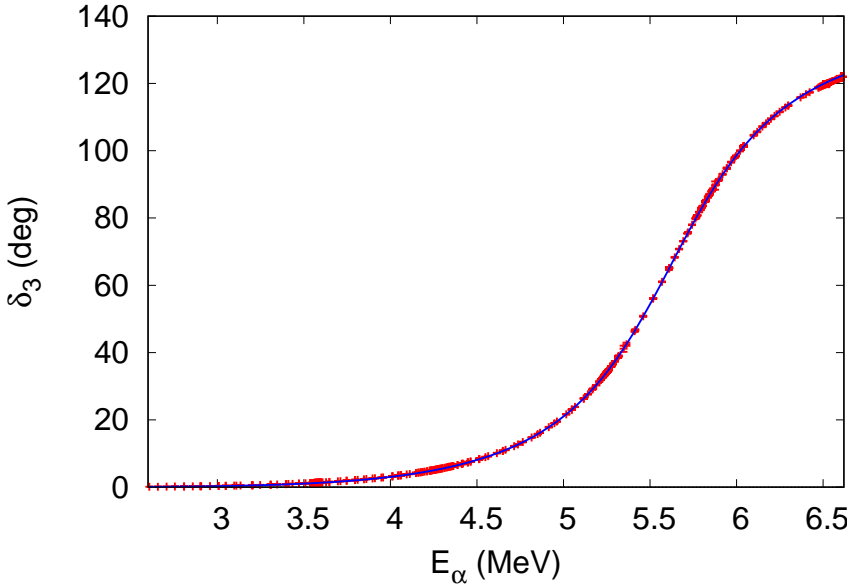


Figure 6: Phase shift δ_3 of elastic α - ^{12}C scattering for f -wave channel as a function of E_α calculated by using the fitted values of the parameters. Experimental data are included in the figure as well.

have $\tilde{R}_3 = -17101/(90720\kappa)$ [24]. When $\tilde{R}_3 > R_3$, a spurious bound state appears below the sub-threshold 3_1^- state of ^{16}O . In addition, we use the experimental values for $E_{R(33)}$ and $\Gamma_{R(33)}$, $E_{R(33)}^{(exp)} = 5.967(10)$ MeV and $\Gamma_{R(33)}^{(exp)} = 110(30)$ keV [37], for the background contribution from high energy. In Table 2, we show fitted values and their errors of the 6 parameters in the amplitudes of the 3_1^+ , 3_2^- , 3_3^- states of ^{16}O in the S matrix of elastic α - ^{12}C scattering for $l = 3$ in Eq. (43) where we find a value of χ^2/N , $\chi^2/N = 0.87$, for the parameter fit, as shown in Table 3. The fitted values of the parameters $a_{(33)}$ and $b_{(33)}$ have large error bars and are not still fitted well because they are insensitive in the parameter fit. While, if we exclude them from the parameter fit, we have a large value of χ^2/N , $\chi^2/N = 1.84$. In Table 4, we show a value of the ANC of the 3_1^- state of ^{16}O ; we have $|C_b| = 113(8)$ fm $^{-1/2}$ which agrees well with our previous estimate, $|C_b| = (1.2\text{--}1.5) \times 10^2$ fm $^{-1/2}$ [24]. In Fig. 6, we plot a curve of the phase shift for $l = 3$, δ_3 , by using the fitted values of the parameters obtained in Table 2. The phase shift data are also displayed in the figure. We find that the fitted curve agrees well with the phase shift data.

4.5 Phase shift for $l = 4$ channel

We consider 4_1^+ , 4_2^+ , 4_3^+ states of ^{16}O to construct the S matrix of elastic α - ^{12}C scattering for $l = 4$ where 4_1^+ and 4_2^+ are the resonant states appearing in the phase shift data at $E_\alpha = 4.26$ MeV and $E_\alpha = 5.25$ MeV, respectively, and 4_3^+ is a resonant state as a

background state from high energy appearing at $E_\alpha = 8.94$ MeV. Thus, we have an expression of the S matrix for $l = 4$ as

$$e^{2i\delta_4} = \prod_{i=1}^3 \frac{E - E_{R(4i)} + R_{(4i)}(E) - i\frac{1}{2}\Gamma_{(4i)}(E)}{E - E_{R(4i)} + R_{(4i)}(E) + i\frac{1}{2}\Gamma_{(4i)}(E)}, \quad (48)$$

with

$$\Gamma_{(4i)}(E) = \Gamma_{R(4i)} \frac{pC_\eta^2 W_4(p)}{p_r C_{\eta_r}^2 W_4(p_r)}, \quad (49)$$

$$R_{(4i)}(E) = a_{(4i)}(E - E_{R(4i)})^2 + b_{(4i)}(E - E_{R(4i)})^3, \quad i = 1, 2, 3 \quad (50)$$

where $p_r = \sqrt{2\mu E_{(4i)}}$. We have 8 parameters to fit to the data as

$$\theta_4 = \{E_{R(41)}, \Gamma_{R(41)}, a_{(41)}, b_{(41)}, E_{R(42)}, \Gamma_{R(42)}, a_{(43)}, b_{(43)}\}, \quad (51)$$

where two parameters $a_{(42)}$ and $b_{(42)}$ are set to be zero, $a_{(42)} = b_{(42)} = 0$, because of their insensitivity for the parameter fit, and we use the experimental values for $E_{R(43)}$ and $\Gamma_{R(43)}$, $E_{R(33)}^{(exp)} = 6.707(20)$ MeV and $\Gamma_{R(33)}^{(exp)} = 89(2)$ keV [37], for the background contribution from high energy.

In Table 2, we show fitted values and their errors of the 8 parameters in the amplitudes of the $4_1^+, 4_2^+, 4_3^+$ states of ^{16}O in the S matrix of elastic α - ^{12}C scattering for $l = 4$ in Eq. (48) where we find a small value of χ^2/N , $\chi^2/N = 0.47$, for the parameter fit, as shown in Table 3. In addition, the fitted values of $E_{R(41)}$, $\Gamma_{R(41)}$, $E_{R(42)}$, and $\Gamma_{R(42)}$ agree with their experimental values, $E_{R(41)}^{(exp)} = 3.194(3)$ MeV, $\Gamma_{R(41)}^{(exp)} = 26(3)$ keV, $E_{R(42)}^{(exp)} = 3.9347(17)$ MeV, and $\Gamma_{R(42)}^{(exp)} = 0.28(5)$ keV [37]. In Fig. 7, we plot a curve of the phase shift for $l = 4$, δ_4 , by using the fitted values of the parameters obtained in Table 2. The phase shift data are also displayed in the figure. We find that the fitted curve agrees well with the phase shift data.

4.6 Phase shift for $l = 5$ channel

We consider 5_1^- state of ^{16}O to construct an S matrix of the elastic α - ^{12}C scattering for $l = 5$ where 5_1^- is a resonant state as a background contribution from high energy appearing at $E_\alpha = 10.00$ MeV. Thus, we have an expression of the S matrix for $l = 5$ as

$$e^{2i\delta_5} = \frac{E - E_{R(51)} + R_{(51)}(E) - i\frac{1}{2}\Gamma_{(51)}(E)}{E - E_{R(51)} + R_{(51)}(E) + i\frac{1}{2}\Gamma_{(51)}(E)}, \quad (52)$$

with

$$\Gamma_{(51)}(E) = \Gamma_{R(51)} \frac{pC_\eta^2 W_5(p)}{p_r C_{\eta_r}^2 W_5(p_r)}, \quad (53)$$

$$R_{(51)}(E) = a_{(51)}(E - E_{R(51)})^2 + b_{(51)}(E - E_{R(51)})^3, \quad (54)$$

where $p_r = \sqrt{2\mu E_{(51)}}$. We have 2 parameters to fit the data as

$$\theta_4 = \{a_{(51)}, b_{(51)}\}, \quad (55)$$

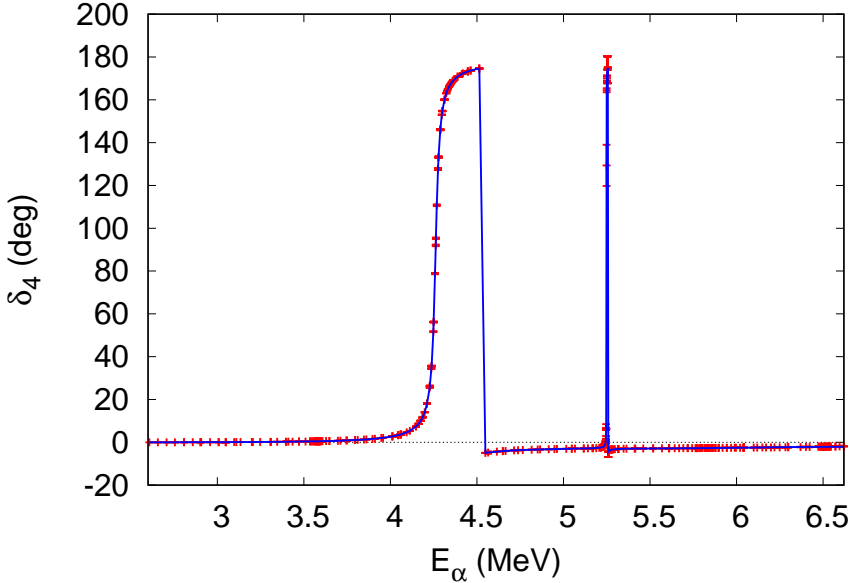


Figure 7: Phase shift δ_4 of elastic α - ^{12}C scattering for g -wave channel as a function of E_α calculated by using the fitted values of the parameters. Experimental data are included in the figure as well.

where we use the experimental values for $E_{R(51)}$ and $\Gamma_{R(51)}$, $E_{R(51)}^{(exp)} = 7.498(2)$ MeV and $\Gamma_{R(51)}^{(exp)} = 670(15)$ keV [37], for the background contribution from high energy.

In Table 2, we show fitted values and their errors of the 2 parameters in the amplitudes of the 5_1^- state of ^{16}O in the S matrix of elastic α - ^{12}C scattering for $l = 5$ in Eq. (52) where we find a very small value of χ^2/N , $\chi^2/N = 0.094$, for the parameter fit, as shown in Table 3. In Fig. 8, we plot a curve of the phase shift for $l = 5$, δ_5 , by using the fitted values of the parameters obtained in Table 2. The phase shift data are also displayed in the figure. We find that the fitted curve agrees well with the phase shift data.

4.7 Phase shift for $l = 6$ channel

We include a background contribution from low energy and the 6_1^+ state of ^{16}O to construct an S matrix of the elastic α - ^{12}C scattering for $l = 6$ where 6_1^+ is a resonant state as a background contribution from high energy appearing at $E_\alpha = 10.20$ MeV. Thus, we have an expression of the S matrix for $l = 6$ as

$$e^{2i\delta_6} = \frac{K_6(p) - 2\kappa \text{Re}H_6(p) + ipC_\eta^2W_6(p)}{K_6(p) - 2\kappa \text{Re}H_6(p) - ipC_\eta^2W_6(p)} \frac{E - E_{R(61)} + R_{(61)}(E) - i\frac{1}{2}\Gamma_{(61)}(E)}{E - E_{R(61)} + R_{(61)}(E) + i\frac{1}{2}\Gamma_{(61)}(E)}, \quad (56)$$

with

$$K_6(p) = \frac{1}{2}r_6p^2 - \frac{1}{4}P_6p^4, \quad (57)$$

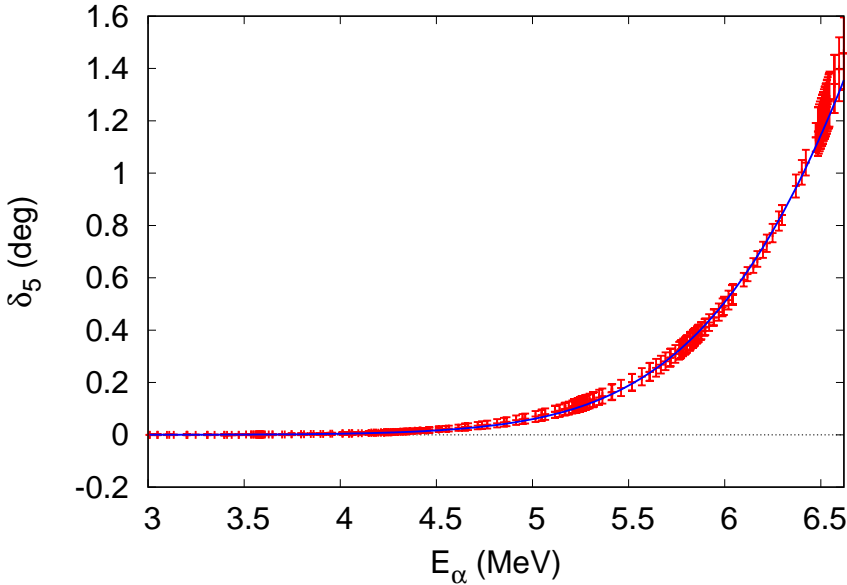


Figure 8: Phase shift δ_5 of elastic α - ^{12}C scattering for h -wave channel as a function of E_α calculated by using the fitted values of the parameters. Experimental data are included in the figure as well.

$$\Gamma_{(61)}(E) = \Gamma_{R(61)} \frac{p C_\eta^2 W_6(p)}{p_r C_{\eta_r}^2 W_6(p_r)}, \quad (58)$$

$$R_{(61)}(E) = a_{(61)}(E - E_{R(61)})^2 + b_{(61)}(E - E_{R(61)})^3, \quad (59)$$

where $p_r = \sqrt{2\mu E_{R(61)}}$. We have four parameters to fit the data as

$$\theta_3 = \{r_6, P_6, a_{(61)}, b_{(61)}\}, \quad (60)$$

where the leading effective range parameter, $-1/a_6$, is put to be zero, $1/a_6 = 0$, and two effective range parameters, r_6 and P_6 , are included while we use the experimental values for $E_{R(61)}$ and $\Gamma_{R(61)}$, $E_{R(61)}^{(exp)} = 7.6534(16)$ MeV and $\Gamma_{R(61)}^{(exp)} = 70(8)$ keV [37], for the background contribution from high energy.

In Table 2, we show fitted values and their errors of the four parameters in the amplitudes of the background contribution from low energy and the 6_1^+ state of ^{16}O in the S matrix of elastic α - ^{12}C scattering for $l = 6$ in Eq. (56) where we find a very small value of χ^2/N , $\chi^2/N = 0.026$, for the parameter fit, as shown in Table 3. In Fig. 9, we plot a curve of the phase shift for $l = 6$, δ_6 , by using the fitted values of the parameters obtained in Table 2. The phase shift data are also displayed in the figure. We find that the fitted curve agrees well with the phase shift data.

5. Results and discussion

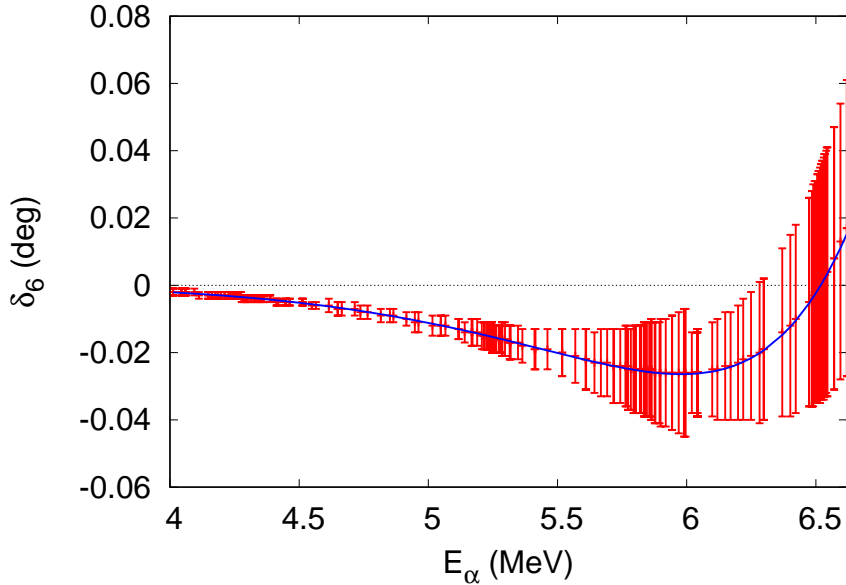


Figure 9: Phase shift δ_6 of elastic α - ^{12}C scattering for i -wave channel as a function of E_α calculated by using the fitted values of the parameters. Experimental data are included in the figure as well.

In the present work, we studied the expression of the S matrices of elastic α - ^{12}C scattering at low energies for $l = 0, 1, 2, 3, 4, 5, 6$ in EFT. The S matrices are constructed as the summation of the phase shifts; the parts of the phase shifts are obtained from the elastic scattering amplitudes of the sub-threshold and resonant states of ^{16}O . Those amplitudes are calculated from the effective Lagrangian and obtained in terms of the effective range parameters up to p^6 order for $l = 0, 1, 2, 4, 5, 6$ and up to p^8 order for $l = 3$ due to the modification of the counting rules for the effective range parameters discussed in Refs. [26, 29]. We include the sub-threshold states for $l = 0, 1, 2, 3$ and a background contribution from low energy for $l = 6$, one resonant state for $l = 0, 1, 3$ and two resonant states for $l = 2, 4$, which appear in the energy range of the phase shift data, $2.6 \text{ MeV} < E_\alpha < 6.62 \text{ MeV}$, and a resonant state which appears at $6.62 \text{ MeV} < E_\alpha$, as background contributions from high energy for all the partial wave states. Those states included in the present study are summarized in Table 1. Then, we fit the parameters to the phase shift data while the resonant energies and widths of the background contributions from high energy are fixed by using the experimental data of the resonant states at $6.62 \text{ MeV} < E_\alpha$, and some parameters which are insensitive to the parameter fit are suppressed. We find that the parameters are fitted very well where the χ^2/N values are less than one for all the cases, as summarized in Table 3, and thus, the phase shifts are well described within the theory.

One may regard this work as merely a simple parameter fit to the phase shift data while our aim is to extrapolate the radiative capture rate down to the Gamow peak energy, $E_G = 0.3$ MeV; one may see that our result is comparable to that worked out by the R -matrix analysis. One may also see that the parameterization based on the effective range expansion in the S matrices in Eq. (27) is simple and transparent. In addition, the electromagnetic and weak interactions are straightforwardly introduced in the theory. As mentioned in the introduction, we employed the EFT to the study of the $E1$ transition of the $^{12}\text{C}(\alpha, \gamma)^{16}\text{O}$ reaction [26] and the β -delayed α -emission from ^{16}N [7].⁴ Recently, we reported the first application of EFT to the study of the radiative proton capture on ^{15}N [49, 50], which is an important reaction in the CNO cycle. Thus, constructing an EFT would be another theoretical method, as an alternative to the R -matrix analysis, for the studies of nuclear reactions for stellar evolution.

Acknowledgements

We would like to thank S. W. Hong, T.-S. Park, and C. H. Hyun for discussions. We also thank the reviewers for the discussions and for providing the data files of wavefunctions and phase shifts calculated from a Woods-Saxon potential. This work was supported by the National Research Foundation of Korea (NRF) grant funded by the Korean government (MSIT) (No. 2019R1F1A1040362 and 2022R1F1A1070060).

Appendix

In the present appendix, we perform a test calculation by employing a Woods-Saxon potential. The data, wavefunctions and phase shifts, are generated by using the model potential, the values of ANC s are calculated from the wavefunctions, and the scattering phase shifts are generated by using the potential. We, then, fit the effective range parameters to the phase shift data generated from the potential, and calculate the ANC s by using the fitted values of parameters in Eq. (18). We note that the relation between the two methods, the potential model and the effective range expansion, to deduce the ANC s is not obvious. The comparison of the ANC s from the potential model and the fit of effective range parameters may indicate some degree of the model dependence in the two methods.

In Figs. 10 and 11, we display the wavefunctions of the 0^+ and 2^+ states of ^{16}O , respectively, from a Woods-Saxon potential. The geometry of Woods-Saxon potential is standard; $R_0 = 1.3$ fm; $R = R_0 A^{1/3} = 2.976$ fm and $a = 0.7$ fm. The wavefunctions of bound states are obtained by adjusting the depth of potential. For the 0^+ state, $E_x = 6049.4$ keV and $B_0 = 1112.5$ keV, and one has $V_0 = 131.1$ MeV, and for the 2^+ state, $E_x = 6917.1$ keV and $B_2 = 244.8$ keV, and one has $V_0 = 130.8$ MeV. The wavefunctions are normalized as $\int_0^\infty u_l(r)^2 dr = 1$ with $l = 0, 2$. (The data files of wavefunctions and phase shifts are provided by a reviewer.)

⁴The dressed propagators of ^{16}O shown in Fig. 1, $D_l^{-1}(p)$ for $l = 1$ and $l = 3$, whose parameters are fitted to the phase shift data, are used as the building blocks of reaction amplitudes of the $E1$ transition of $^{12}\text{C}(\alpha, \gamma)^{16}\text{O}$ and the β -delayed α -emission of ^{16}N .

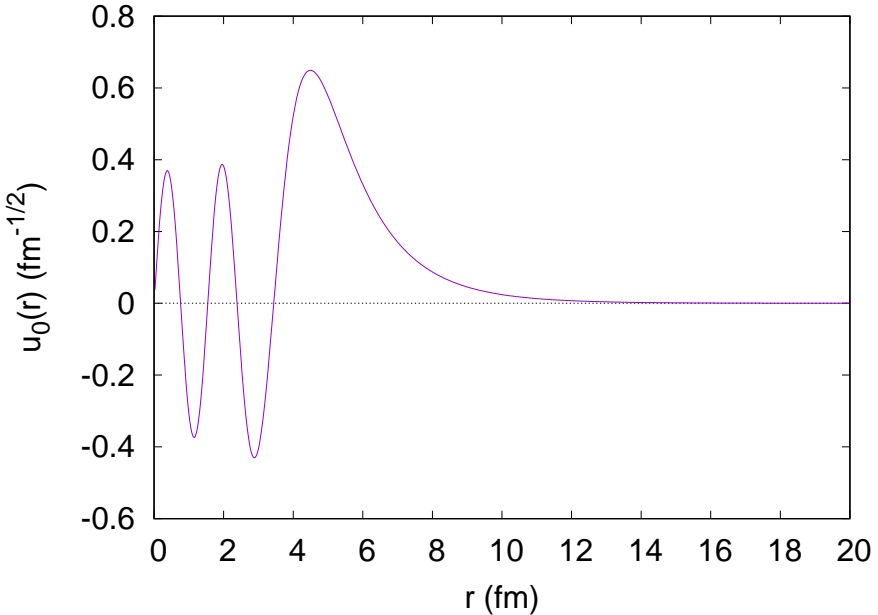


Figure 10: Wavefunction for 0^+ state of ^{16}O calculated by using a Woods-Saxon potential, which is normalized as $\int_0^\infty u_0(r)^2 dr = 1$.

The values of ANCs may be obtained by using the relations

$$u_0(r) \sim |C_b|_0 W_{-\kappa/\gamma_0, \frac{1}{2}}(2\gamma_0 r), \quad u_2(r) \sim |C_b|_2 W_{-\kappa/\gamma_2, \frac{5}{2}}(2\gamma_2 r), \quad (61)$$

at the outside of the potential range, $R < r$, where $W_{\nu, \mu}(z)$ is the Whittaker function, and γ_0 and γ_2 are the binding momenta, $\gamma_0 = \sqrt{2\mu B_0}$ and $\gamma_2 = \sqrt{2\mu B_2}$. Thus, we have the ANCs from the wavefunctions as

$$|C_b|_0 = 2.6 \times 10^3 \text{ fm}^{-1/2}, \quad |C_b|_2 = 1.9 \times 10^5 \text{ fm}^{-1/2}. \quad (62)$$

It is good to see that the ANCs are straightforwardly obtained from the wavefunctions generated from the potential model after fitting the depth of potential to the binding energies. While one may wonder about the sensitivity of ANCs to all the three parameters of potential and the number of nodes of wavefunctions inside the potential range. In addition, the ANCs from the potential model depend on the normalization condition of wavefunctions; the reliability of two-body description of the 16-body nucleon system inside the potential range is questionable.

In Figs. 12 and 13, we display the phase shifts of elastic α - ^{12}C scattering for $l = 0$ and 2, respectively, calculated from the Woods-Saxon potential with the fixed values of V_0 mentioned above. Now we carry out a test for our fitting method to deduce the ANCs from the phase shift data: the effective range parameters are fitted to the phase shift data in the figures, and we calculate the ANCs by using Eq. (18). When fitting the phase shift

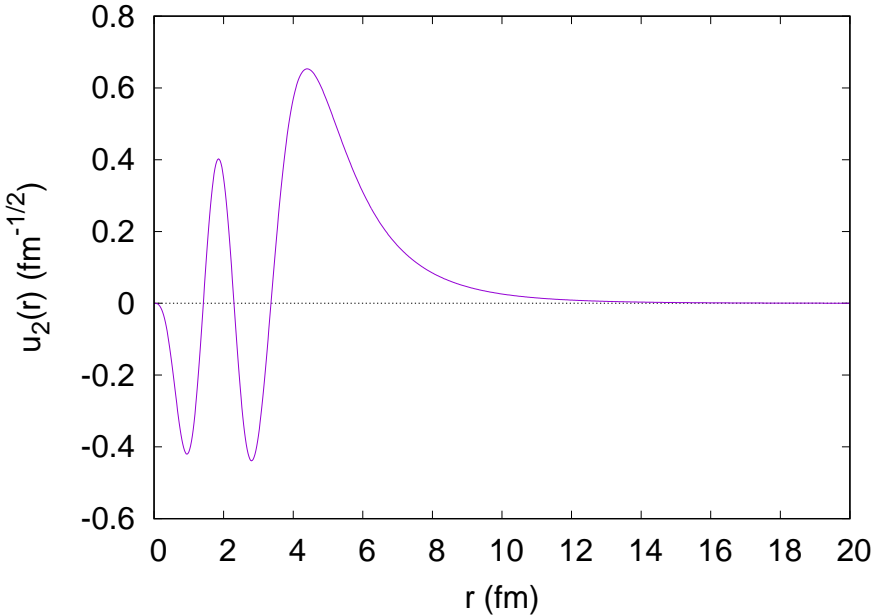


Figure 11: Wavefunction for 2^+ state of ^{16}O calculated by using a Woods-Saxon potential, which is normalized as $\int_0^\infty u_2(r)^2 dr = 1$.

data, we include a constant error to the phase shift data, $\Delta\delta_{0,2} = 0.20$ degree, which is a typical size of the error in the phase shift data for $l = 0$ from the experiment.

In Table 5, we display the values of ANC for the 0^+ state as a function of the maximum energy, $E_{\alpha,max} = 4.0, 4.5, 5.0, 5.5$ MeV, of the phase shift data in Fig. 12. We find that the shapes of the curves of the phase shift are different (the curve from the effective range parameters is stiffer than that from the potential model), and it leads to the energy dependence of the fit.⁵ One can see that the values of ANC in the table have a significant range, $(1.1\text{--}5.8) \times 10^3 \text{ fm}^{-1/2}$ with $\chi^2/N = 0.05\text{--}1.18$, while the ANC from the potential model, $2.6 \times 10^3 \text{ fm}^{-1/2}$, can be found within the range of ANC from the fit. For the 2^+ state, using all the phase shift data in Fig. 13, we have

$$|C_b|_2 = 3.4(54.4) \times 10^5 \text{ fm}^{-1/2}, \quad (63)$$

with $\chi^2/N = 0.13$. The center value of ANC is 1.8 times larger than that of the potential model in Eq. (61) while the ANC from fit has a large error bar. As discussed in Ref. [29], when the center value of dD/dp^2 term at $p = i\gamma_2$ almost vanishes in the denominator in Eq. (18), the error of ANC is enhanced.

In this appendix, we performed a test calculation to study whether the ANCs obtained from the wavefunctions of a potential model can be reproduced by fitting the effective

⁵The different energy dependence in the phase shifts possibly came out due to the use of an energy-independent potential model, where one may notice that the calculated phase shifts do not agree with the experimental data. The use of an energy-dependent potential could improve the present situation.

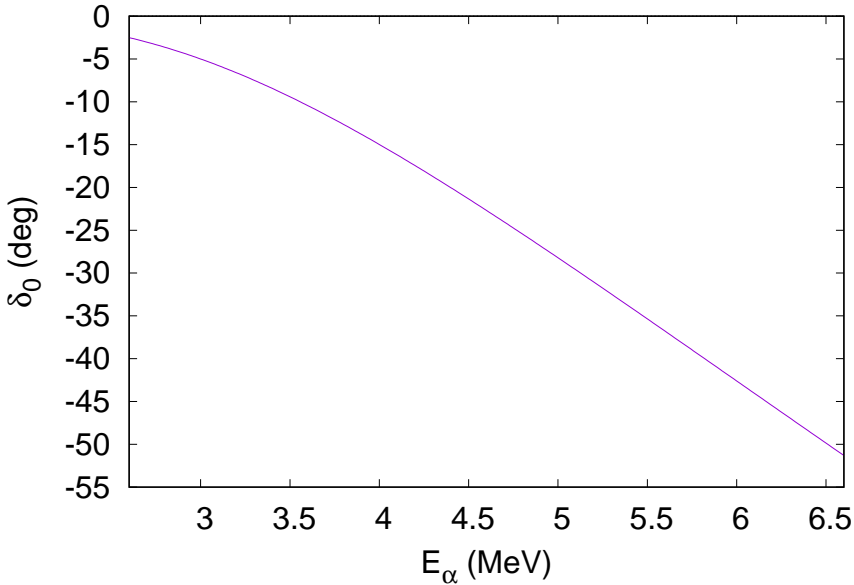


Figure 12: Phase shift δ_0 of elastic α - ^{12}C scattering for $l = 0$ as a function of the α energy E_α in the lab mass frame, calculated by using a Woods-Saxon potential.

range parameters to the phase shift generated by the model potential. We find that the ANCs obtained from the fitted values of effective range parameters agree with those obtained from the wavefunction of the potential model within the uncertainties discussed above; aside from the large uncertainties, the center values of ANCs agree within a factor of 2. The large uncertainties may stem from the formula of ANC in Eq. (18). When the slope of the inverse of the propagator, $D_l(p)$, becomes small at the binding momentum $p = i\gamma_l$, the ANC becomes large. In other words, the center value of ANC becomes sensitive to the values of effective range parameters while the errors of ANC are enhanced. Therefore, because of the difficulty discussed above, the present cases to deduce the ANCs of 0^+ and 2^+ state from the phase shift data may not be ideal: the uncertainty of a factor of 2 may be involved between the two methods.

References

- [1] W. A. Fowler, Rev. Mod. Phys. **56**, 149 (1984).
- [2] L. R. Buchmann and C. A. Barnes, Nucl. Phys. A **777**, 254 (2006).
- [3] A. Coc, F. Hammache, J. Kiener, Eur. Phys. J. A **51**, 34 (2015).
- [4] C. A. Bertulani and T. Kajino, Prog. Part. Nucl. Phys. **89**, 56 (2016).

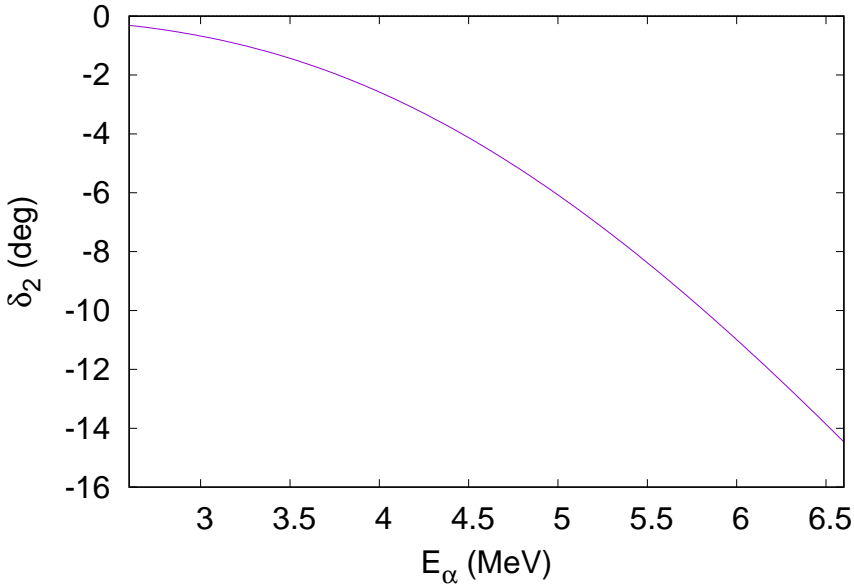


Figure 13: Phase shift δ_2 of elastic α - ^{12}C scattering for $l = 2$ as a function of the α energy E_α in the lab frame, calculated by using a Woods-Saxon potential.

- [5] R. J. deBoer *et al.*, Rev. Mod. Phys. **89**, 035007 (2017), and references therein.
- [6] H.-W. Hammer, S. König, and U. van Kolck, Rev. Mod. Phys. **92**, 25004 (2020).
- [7] S.-I. Ando, Eur. Phys. J. A **57**, 17 (2021).
- [8] R. Plaga *et al.*, Nucl. Phys. A **465**, 291 (1987).
- [9] P. Tischhauser *et al.*, Phys. Rev. C **79**, 055803 (2009).
- [10] S. Weinberg, Physica A **96**, 327 (1979).
- [11] P. F. Bedaque and U. van Kolck, Ann. Rev. Nucl. Part. Sci. **52**, 339 (2002).
- [12] D. B. Kaplan, Nucl. Phys. B **494**, 471 (1997).
- [13] S. R. Beane and M. J. Savage, Nucl. Phys. A **694**, 511 (2001).
- [14] S. Ando and C. H. Hyun, Phys. Rev. C **72**, 014008 (2005).
- [15] H. A. Bethe, Phys. Rev. **76**, 38 (1949).
- [16] J. W. Chen and M. J. Savage, Phys. Rev. C **60**, 065205 (1999).
- [17] G. Rupak, Nucl. Phys. A **678**, 405 (2000).

- [18] S. Ando, R. H. Cyburt, S. W. Hong, and C. H. Hyun, Phys. Rev. C **74**, 025809 (2006).
- [19] X. Kong and F. Ravndal, Nucl. Phys. A **656**, 421 (1999).
- [20] M. Butler and J.-W. Chen, Phys. Lett. B **520**, 87 (2001).
- [21] S. Ando et al., Phys. Lett. B **668**, 187 (2008).
- [22] M. Butler, J.-W. Chen, and X. Kong, Phys. Rev. C **63**, 035501 (2001).
- [23] S.-I. Ando, Y.-H. Song, and C. H. Hyun, Phys. Rev. C **101**, 054001 (2020).
- [24] S.-I. Ando, Phys. Rev. C **97**, 014604 (2018).
- [25] S.-I. Ando, Eur. Phys. J. A **52**, 130 (2016).
- [26] S.-I. Ando, Phys. Rev. C **100**, 015807 (2019).
- [27] B. Gelman, Phys. Rev. C **80**, 034005 (2009).
- [28] J. B. Habashi, S. Fleming, and U. van Kolck, Eur. Phys. J. A **57**, 169 (2021).
- [29] S.-I. Ando, Phys. Rev. C **105**, 064603 (2022).
- [30] J. J. Sakurai, "Modern Quantum Mechanics." Addison-Wesley; revised edition (August 31, 1993).
- [31] J. Jerphagnon, Phys. Rev. B **2**, 1091 (1970).
- [32] D. L. Andrews and W. A. Ghoul, Phys. Rev. A **25**, 2647 (1982).
- [33] H. W. Grießhammer, Nucl. Phys. A **744**, 192 (2004).
- [34] Z. R. Iwinski, L. Rosenberg, and L. Spruch, Phys. Rev. C **29**, 349 (1984).
- [35] R. Higa, H.-W. Hammer, and U. van Kolck, Nucl. Phys. A **809**, 171 (2008).
- [36] D. Foreman-Mackey et al., Pub. Astro. Soc. Pac. **125**, 306 (2013).
- [37] D. R. Tilley, H. R. Weller, and C. M. Cheves, Nucl. Phys. A **564**, 1 (1993).
- [38] S.-I. Ando, Phys. Rev. C **102**, 034611 (2020).
- [39] D. Schürmann et al., Phys. Lett. B **703**, 557 (2011).
- [40] R. deBoer et al., Phys. Rev. C **87**, 015802 (2013).
- [41] M. L. Avila et al., Phys. Rev. Lett. **114**, 071101 (2015).

- [42] L. D. Blockhintsev, A. S. Kadyrov, A. M. Mukhamedzhanov, and D. A. Savin, Phys. Rev. C **97**, 024602 (2018).
- [43] L. D. Blockhintsev, A. S. Kadyrov, A. M. Mukhamedzhanov, and D. A. Savin, Eur. Phys. J. A **58**, 257 (2022).
- [44] Yu. V. Orlov, B. F. Irgaziev, and J.-U. Nabi, Phys. Rev C **96**, 025809 (2017).
- [45] Yu. V. Orlov, Nucl. Phys. A **1014**, 122257 (2021); Erratum, Nucl. Phys. A **1018**, 122385 (2022).
- [46] C. R. Brune, W. H. Geist, R. W. Kavanagh, and K. D. Veal, Phys. Rev. Lett. **83**, 4025 (1999).
- [47] A. Belhout et al., Nucl. Phys. A **793**, 178 (2007).
- [48] S. Adhikari and C. Basu, Phys. Lett. B **682**, 216 (2009).
- [49] S. Son, S.-I. Ando, and Y. Oh, New Phys.: Sae Mulli **72**, 291 (2022).
- [50] S. Son, S.-I. Ando, and Y. Oh, Phys. Rev. C **106**, 055807 (2022).

l_{i-th}^π	p^0 order	p^2	p^4	p^6	p^8
0_2^+	$a_0(\text{fm})$ —	$r_0(\text{fm})$ 0.26847(1)	$P_0(\text{fm}^3)$ −0.0363(4)	$Q_0(\text{rm}^5)$ 0.0011(1)	
0_3^+	$E_{R(03)}(\text{MeV})$ 4.8884(1)	$\Gamma_{R(03)}(\text{keV})$ 1.34(3)			
0_4^+	$E_{R(04)}(\text{MeV})$ —	$\Gamma_{R(04)}(\text{keV})$ —	$a_{(04)}(\text{MeV}^{-1})$ 0.75(1)	$b_{(04)}(\text{MeV}^{-2})$ 0.18(1)	
$1_1^-, 1_2^-$	$a_1(\text{fm}^3)$ —	$r_1(\text{fm}^{-1})$ 0.415314(7)	$P_1(\text{fm})$ −0.57428(7)	$Q_1(\text{fm}^3)$ 0.02032(2)	
1_3^-	$E_{R(13)}(\text{MeV})$ —	$\Gamma_{R(13)}(\text{keV})$ —	$a_{(13)}(\text{MeV}^{-1})$ 0.43(25)	$b_{(13)}(\text{MeV}^{-2})$ 3.8(7)	
2_1^+	$a_2(\text{fm}^5)$ —	$r_2(\text{fm}^{-3})$ 0.149(4)	$P_2(\text{fm}^{-1})$ −1.19(5)	$Q_2(\text{fm})$ 0.081(16)	
2_2^+	$E_{R(22)}(\text{MeV})$ 2.68308(5)	$\Gamma_{R(22)}(\text{keV})$ 0.75(2)			
2_3^+	$E_{R(23)}(\text{MeV})$ 4.3545(2)	$\Gamma_{R(23)}(\text{keV})$ 74.61(3)	$a_{(23)}(\text{MeV}^{-1})$ 0.46(12)	$b_{(23)}(\text{MeV}^{-2})$ 0.49(9)	
2_4^+	$E_{R(24)}(\text{MeV})$ —	$\Gamma_{R(24)}(\text{keV})$ —			
$3_1^-, 3_2^-$	$a_3(\text{fm}^7)$ —	$r_3(\text{fm}^{-5})$ 0.0335(2)	$P_3(\text{fm}^{-3})$ −0.446(9)	$Q_3(\text{fm}^{-1})$ 0.311(5)	$R_3(\text{fm})$ −0.152(3)
3_3^-	$E_{R(33)}(\text{MeV})$ —	$\Gamma_{R(33)}(\text{keV})$ —	$a_{(33)}(\text{MeV}^{-1})$ 32(32)	$b_{(33)}(\text{MeV}^{-2})$ 3.2(32) $\times 10^2$	
4_1^+	$E_{R(41)}(\text{MeV})$ 3.19606(1)	$\Gamma_{R(41)}(\text{keV})$ 25.91(1)	$a_{(41)}(\text{MeV}^{-1})$ 0.740(3)	$b_{(41)}(\text{MeV}^{-2})$ 0.304(5)	
4_2^+	$E_{R(42)}(\text{MeV})$ 3.93655(2)	$\Gamma_{R(42)}(\text{keV})$ 0.425(4)			
4_3^+	$E_{R(41)}(\text{MeV})$ —	$\Gamma_{R(41)}(\text{keV})$ —	$a_{(43)}(\text{MeV}^{-1})$ 0.889(6)	$b_{(43)}(\text{MeV}^{-2})$ 0.216(3)	
5_1^-	$E_{R(51)}(\text{MeV})$ —	$\Gamma_{R(51)}(\text{keV})$ —	$a_{(51)}(\text{MeV}^{-1})$ 0.572(6)	$b_{(51)}(\text{MeV}^{-2})$ 0.104(2)	
(bg)		$r_6(\text{fm}^{-11})$ −0.3(2)	$P_6(\text{fm}^{-9})$ 2(1)		
6_1^+	$E_{R(61)}(\text{MeV})$ —	$\Gamma_{R(61)}(\text{keV})$ —	$a_{(61)}(\text{MeV}^{-1})$ 0.8(1)	$b_{(61)}(\text{MeV}^{-2})$ 0.18(4)	

Table 2: Fitted values of the parameters in the amplitudes of the sub-threshold and resonant states of ^{16}O (and a background contribution for $l = 6$), which are listed in table 1, in the S matrices of elastic α - ^{12}C scattering for $l = 0, 1, 2, 3, 4, 5, 6$. The parameters whose values are not shown in the table are fixed by using the experimental data. Parameters not shown in the table are not included in the parameter fit.

l	0	1	2	3	4	5	6
χ^2/N	0.013	0.089	0.66	0.87	0.47	0.094	0.026

Table 3: Values of χ^2/N for $l = 0, 1, 2, 3, 4, 5, 6$ for the parameter fit where $N = 252$ for $l = 0, 1, 2, 3, 4$, $N = 243$ for $l = 5$, and $N = 186$ for $l = 6$.

l_{i-th}^π	0_2^+	1_1^-	2_1^+	3_1^-
$ C_b (\text{fm}^{-1/2})$	370(25)	$1.727(3) \times 10^{14}$	$3.1(6) \times 10^4$	113(8)

Table 4: Values of ANC, $|C_b|$, for the sub-threshold 0_2^+ , 1_1^- , 2_1^+ , 3_1^- states of ^{16}O .

$E_{\alpha,max}$ (MeV)	4.0	4.5	5.0	5.5
$ C_b _0$ ($\text{fm}^{-1/2}$)	1.1×10^3	2.2×10^3	3.7×10^3	5.8×10^3
χ^2/N	0.05	0.16	0.43	1.18

Table 5: ANC of 0^+ state, $|C_b|_0$, as a function of the maximum energy of the data, $E_{\alpha,max}$ (MeV), deduced from the phase shift data in Fig. 12. Values of χ^2/N are also displayed in the table.